International Journal of Applied Earth Observations and Geoinformation 110 (2022) 102809

Contents lists available at ScienceDirect

International Journal of Applied Earth Observations and Geoinformation

journal homepage: www.elsevier.com/locate/jag

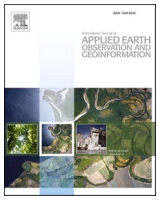

Coupling remote sensing and particle tracking to estimate trajectories in large water bodies

Chaojie Li [a], Daniel Odermatt [b,*], Damien Bouffard [c], Alfred Wüest [c,d], Tamar Kohn [a,*]

[a] Laboratory of Environmental Chemistry, School of Architecture, Civil & Environmental Engineering (ENAC), École Polytechnique Fédérale de Lausanne, Lausanne 1015, Switzerland
[b] Eawag, Swiss Federal Institute of Aquatic Science and Technology, Surface Waters – Research and Management, 8600 Dübendorf, Switzerland
[c] Eawag, Swiss Federal Institute of Aquatic Science and Technology, Surface Waters – Research and Management, 6047 Kastanienbaum, Switzerland
[d] Physics of Aquatic Systems Laboratory (APHYS) Margaretha Kamprad Chair, ENAC, EPFL, 1015 Lausanne, Switzerland

ARTICLE INFO

Keywords:
Water quality modelling
Particle tracking
Remote sensing
Sentinel
Total suspended matter

ABSTRACT

Propelled by the rapid development of equipment, technology and computational power, the monitoring and simulation of the hydrodynamics in lakes have steadily advanced. In contrast, water quality simulations are more difficult to implement, due to the difficulty in obtaining large-scale, spatially resolved field observations for model validation and the number of interacting processes to be parameterized. Here we demonstrate that remote sensing data can be used to inform Lagrangian particle tracking in a large lake, and vice versa. We used total suspended matter (TSM) as a parameter that can be both estimated from the backscattering in satellite images and modelled in terms of particle abundance. Specifically, we compared TSM concentrations in Lake Geneva deduced from images taken by Sentinel-2 and Sentinel-3 satellites to those estimated from Delft3D hydrodynamic and particle tracking models. TSM concentrations obtained from both methods were compared over a time span of up to 5 days in several scenario studies, including instantaneous and continuous point sources and large-scale TSM simulations. The results demonstrate that remote sensing images can serve to calibrate and validate particle tracking models with independent observations. The model was able to capture both the position of a TSM cloud arising 5 days after an instantaneous point source release, and the direction of particle transport and TSM plume size resulting from a continuous source. Even when simulating the whole lake domain, model results closely approximated the satellite-derived TSM concentrations along lake transects within 9%. In return, the particle tracking model was able to complete partially impaired satellite images, and fill in a four-day image gaps between satellite revisits. The synergy of remote sensing techniques and particle tracking modelling allows a rapid, continuous and more accurate analysis on solute transport in lakes.

1. Introduction

With ~ 3.3% of the earth's land area (Verpoorter et al., 2014), lakes cover only a small part of the globe. Yet, they are essential and easily accessible sources of drinking water and home to a diverse flora and fauna. Lake management requires monitoring and assessing how physical, chemical and biological processes interact (Bonnet et al., 2000). To understand and predict the functioning of lakes is a challenging task due to their high heterogeneity and the complex boundary conditions. However, technologies involving in-situ monitoring, hydrodynamic and water quality models and remote sensing observations can greatly facilitate this task (Kiefer et al., 2015).

Field measurements of water quality parameters have been long employed as the only tool for lake monitoring. While field measurements can capture a wide variety of water quality parameters and remain an absolute reference for other methods, they are often limited in spatial and temporal resolution (Gholizadeh et al., 2016). In contrast, remote sensing images provide an extensive spatial coverage with minimum effort and in a timely manner, and various algorithms are available for estimating different water quality parameters from such imagery (Odermatt et al., 2012). Satellite images are therefore increasingly used for surface water monitoring of lakes (Kiefer et al., 2015) and large reservoirs (Watanabe et al., 2018). But due to the optical complexity of lakes and rivers, and of the overlaying local atmosphere, remote sensing of inland water bodies is more challenging than for oceans (Dörnhöfer and Oppelt, 2016). Depending on spatial

* Corresponding authors.
E-mail addresses: daniel.odermatt@eawag.ch (D. Odermatt), tamar.kohn@epfl.ch (T. Kohn).

https://doi.org/10.1016/j.jag.2022.102809
Received 4 October 2021; Received in revised form 20 April 2022; Accepted 30 April 2022

resolution requirements, both ocean colour (SeaWiFS, MODIS, MERIS) and land colour satellite sensors (Landsat MSS/TM/OLI) can be used for lake monitoring. The former is advantageous for applications requiring high spectroradiometric resolution, e.g. using pigment absorption features, while the latter can resolve optically prominent features at smaller scales (Nouchi et al., 2019). Recently, the European Space Agency and the European Union launched the first generation of the Copernicus Earth observation constellation (formerly GMES; Aschbacher and Milagro-Pérez, 2012). It comprises, among others, of two Sentinel-2 satellites with 10 to 60 m spatial resolution and 5-day joint revisit time (Drusch et al., 2012) and two Sentinel-3 satellites with 300 m spatial resolution and daily joint revisit (Donlon et al., 2012) for land and ocean monitoring, respectively.

While remote sensing is particularly powerful in monitoring the surface layer of lakes (Lehmann et al., 2021), numerical modelling provides a convenient tool to evaluate the dynamics of the entire lake and to rationalize any remotely observed spatial variability (Bouffard et al., 2018; Curtarelli et al., 2014; Soulignac et al., 2018; Wynne et al., 2013). It is thus sensible to couple remote sensing with numerical simulation to merge the advantages of each individual method. The most common coupled application consists in assimilating remotely sensed data to improve numerical models of hydrodynamics or water quality (Allan et al., 2016; Baracchini et al., 2020a; Chen et al., 2010; Stroud et al., 2009; Thomas et al., 2020). Most such models are based on the conventional Eulerian method, which is convenient for the incorporation of boundary conditions and efficient in solving tracer dynamics (Platzek et al., 2014). This approach is interesting to study volume-based quantities such as concentration, but individual fluid particles are not identified. Alternatively, a combination of remote sensing and numerical modelling may be applied using a Lagrangian approach. Lagrangian particle tracking methods have the advantage of strict conservation of mass, avoidance of numerical dispersion and easy incorporation of self-movement of simulated particles or flow-independent processes such as particle growth or decay. They are already widely employed in ocean and atmospheric research with, for instance, spectacular success in tracking oil spills in the Gulf of Mexico during the Deepwater catastrophe (Liu et al., 2011) or emissions of banned ozone-depleting substances (Park et al., 2021). While particle tracking methods are also established tools in limnology (Hoyer et al., 2015; Piccolroaz et al., 2019; Razmi et al., 2014), the combination of particle tracking models with remote sensing products remains limited to a few applications (Xue et al., 2017) and requires further assessment.

In this study, we propose a Lagrangian particle tracking model that interplays with remote sensing techniques to yield synergistic information from simulations and observations. The particle tracking model can be supported and validated by remote sensing results and, in return, provides the possibility for data inference and interpolation between satellite images. The synergy of both methods can comprehensively facilitate the understanding of transport processes in lakes, as both methods benefit from each other. We use Lake Geneva, located on the border of Switzerland and France, as our study site. Lake Geneva is the largest freshwater lake in Western Europe. It has a surface area of 580 km^2 and 89 km^3 of volume, with a maximum depth of ~ 310 m. The lake is used as a drinking water source by more than 800,000 people and appreciated as a recreational site. The complex nature and the important role of this lake make it an attractive site for research studies (Wüest et al., 2021). We first adapted a previously published and fully validated hydrodynamic model of the lake (Baracchini et al., 2020b), and coupled it with a particle tracking module. Then, the particle tracking module was validated using satellite remote sensing data products. Finally, we assessed the advantages and potential uses of the combined particle tracking-remote sensing approach.

2. Material and methods

2.1. Hydrodynamic flow and particle modelling

Delft3D, an open source three-dimensional (3D) hydrodynamic and water quality simulation software, was employed to perform numerical simulations (https://oss.deltares.nl/web/delft3d). Both the hydrodynamic flow and the particle tracking modules were used. The flow model in Delft3D solves the shallow water equations as well as the transport equations in 3D (Deltares, 2015), while the particle tracking module computes particle motions under a Lagrangian framework. The numerical model was set up based on bathymetry samples of Lake Geneva, and the complete initial conditions of the flow and temperature fields were extracted from the existing online open access simulation platform for Lake Geneva (https://meteolakes.ch/; Baracchini et al., 2020). For our simulation, the horizontal z-layer gridding system was converted into a bottom following sigma-gridding system. This coordinate transformation was necessary to allow interfacing with the particle tracking module and to better capture the topography of the beach side of Lake Geneva with a high resolution in shallow regions of the lake.

The hydrodynamic model was set up with 100 layers in the vertical direction, with an average horizontal grid size of 300 × 400 m and a time step of 1 min. The model was driven by various observations as boundary conditions. Major parameters influencing current flow and temperature were of primary interests in this study and were specified and incorporated into the hydrodynamic model. Meteorological inputs were adapted from the COSMO1 data (https://www.meteoswiss.admin.ch). Meteorological parameters included air temperature, air pressure, wind velocity, wind direction, solar radiation, cloudiness and relative humidity. River discharge data as well as turbidity measurements were obtained from the Swiss Federal Office of the Environment (https://www.bafu.admin.ch). Flow time series data were incorporated as boundary conditions at five points: the inlet and outlet of Lake Geneva's main tributary, the Rhône River, and the inlets of three minor tributaries (Dranse, Aubonne and Venoge).

In particle tracking, particle motion is described in a Lagrangian framework (Wilson and Sawford, 1996). In a flow field with given Eulerian velocities, the velocity U consists of a spatially resolved part $\overline{U}$ and a sub-grid part $\widehat{U}$. Total displacement of a particle is the integral of both parts:

$$\Delta X = \int_t^{t+\Delta t} U dt = \int_t^{t+\Delta t} \overline{U} dt + \int_t^{t+\Delta t} \widehat{U} dt = \Delta \overline{X} + \Delta \widehat{X} \tag{1}$$

When the time step Δt is large enough for the particle to ''forget'' its previous velocity, a zero-order model is sufficient in practical applications:

$$\Delta \widehat{X} = \boldsymbol{R} \tag{2}$$

$$\boldsymbol{R} \sim \sqrt{2D\Delta t} \bullet G(0,1) \tag{3}$$

where $\boldsymbol{R}$ is the random displacement of a particle over Δt, D is the diffusion coefficient, and $G(0,1)$ is the standard Gaussian distribution. The zero-order model and the numerical scheme constitutes the basis for the particle tracking module of the Delft3D software (D-WAQ PART) employed for the simulation of particle transport in our study. The horizontal dispersion coefficient D_H is computed as:

$$D_H = at^b \tag{4}$$

where a and b are dimensionless coefficients and t is time. Here t and D_H have the dimensions of [T] and [L^2/T], respectively. In the simulation process, the particle tracking module inherits hydrodynamics from the flow module described above. The velocity from the flow calculation determines the advective term of the particle transport. The diffusive term however, is superimposed on the advection based on the local

condition of the flow.

2.2. Field measurements

Temperature measurements were taken at three observation sites, namely the Buchillon field mast: WGS84 6.39935° E, 46.45840° N, the LéXPLORE platform: WGS84 6.65776° E, 46.50094° N and SHL2: WGS84 6.58872° E, 46.45270° N (Fig. 1). These observations were used as data to calibrate and validate the sigma-layer hydrodynamic model. The SHL2 site provides surface water temperatures and vertical temperature profiles 18 times per year, as well as turbidity profiles. For turbidity measurements the Seapoint Turbidity Meter CTM214 was employed and an averaging filter with a window size of 3 m was applied for outlier removal (Nouchi et al., 2018). Temperature sensors at the Buchillon mast are deployed in 1 and 35 m below the free water surface. The LéXPLORE platform allows vertical temperature profiling from the water surface down to the local bottom of the lake (~100 m depth). All temperature data were collected and errors during recording were excluded. Velocity data were obtained from continuous ADCP measurements at the Buchillon station and the LéXPLORE platform. The velocity time series at the Buchillon mast is measured at 1 m below the water surface while continuous vertical profiles are measured at the LéXPLORE platform. The data was used as reference for model calibration and validation.

2.3. Remote sensing

Remote sensing image data was obtained from the polar-orbiting, sun-synchronous Sentinel-2A and 2B, and Sentinel-3A and 3B satellites. The Sentinel-2 satellites are equipped with the Multi- Spectral Instrument, aimed at monitoring land surfaces (Drusch et al., 2012). The sensor resolves the visible, short-wave infrared and near-infrared parts of the electromagnetic spectrum in 13 bands, with a spatial resolution from 10 to 60 m. Sentinel-3′s main mission goal is to measure sea surface topography, sea and land surface temperature, and ocean surface colour (Donlon et al., 2012). The two Sentinel-3 satellites carry, besides several other Earth Observation instruments, the Ocean and Land Colour Instrument for water quality estimation.

Total suspended matter concentrations (TSM) and turbidity are approximately proportional to particle backscattering and consequently to variations in the magnitude of spectral water-leaving reflectance observed by satellite sensors (Wen et al., 2018; Zhou et al., 2019). TSM and turbidity are known to correspond quite well (Neukermans et al., 2012), but their linear proportionality can vary, primarily with particle size (Foster et al., 1992). We acquired and processed Sentinel-2 level 1C and Sentinel-3 level 1 full resolution data using the Python package SenCast (https://gitlab.com/eawag-rs/sencast). All data available for Lake Geneva were downloaded from CreoDIAS (https://creodias.eu/) and the Copernicus Open Access Hub. Atmospheric correction and water-leaving reflectance retrieval was performed using Polymer v.4.13 (Steinmetz et al., 2011; Steinmetz and Ramon, 2018) and the default vicarious recalibration for OLCI products. Several semi-analytical algorithms for TSM retrieval were applied to both types of input data. Retrievals using the 665 nm band (Vantrepotte et al., 2011) were chosen for further analyses, because Polymer produced less negative reflectance and artefacts related to adjacency effects than for the longer wavelengths used by other algorithms. A comparison of remotely sensed TSM from Sentinel-3 and in situ measured turbidity at SHL2 (0–10 m average) in the years 2017–2018, as well as more detailed information on the performance of the remote sensing TSM retrieval, is shown in the Supplemental Information (Fig. S1).

2.4. Calibration and validation of the sigma-layer hydrodynamic model

Processed temperature data at the three major monitoring stations in Lake Geneva (Fig. 1), along with velocity measurements at the Buchillon field station and the LéXPLORE platform from 2018 to March 2019, were used for model calibration. The parameters calibrated were the bottom roughness (Z_0), the horizontal eddy viscosity (C_{HV}), the horizontal eddy diffusivity (C_{HD}) and the wind drag coefficients, using a trial and error method. The model set-up and parameterization were validated against temperature and velocity measurements from three weekly measurements in April 2019, June 2019 and August 2019.

2.5. Calibration and validation of the particle tracking model

The particle tracking model was calibrated with satellite images acquired in March to mid-April and July to September 2019. Validation was done using scenario studies with satellite images acquired during periods in 2019 that were not included in the model calibration. Three validation scenarios were applied:

Instantaneous TSM point source, tracking a high concentration patch in the middle part of the lake (June 24 to 29, 2019).

Continuous TSM point source from the Rhône River, with two days of release of TSM according to the turbidity measurement at the Rhône River inlet (June 28 to 29, 2019).

Simulation of TSM in the whole lake domain (April 15 to 20, 2019).

For the first scenario, a high concentration patch of TSM was

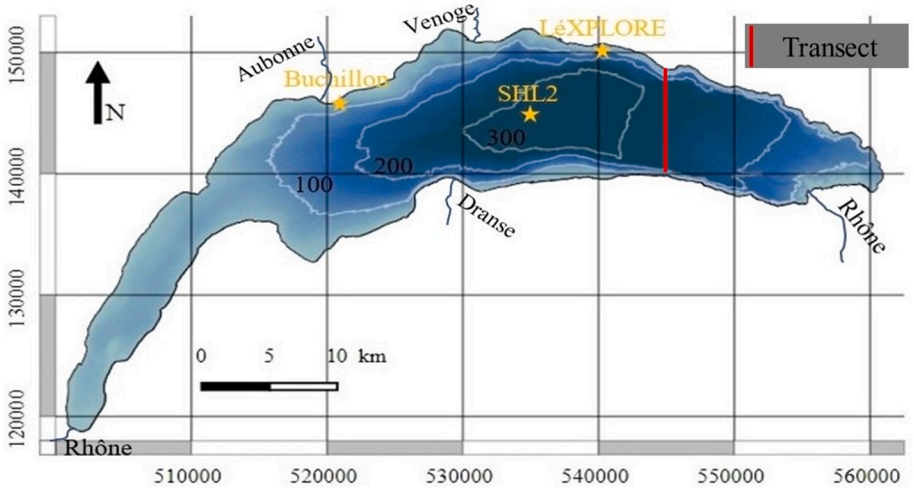

Fig. 1. Map of Lake Geneva and the observation platforms that delivered temperature and velocity data used in the calibration and validation of the hydrodynamic model. Also shown (red line) is the position of the virtual sampling transect used in this work.

identified in the open water of the lake (between 6.462° E and 6.853° E) using remote sensing imagery. We then compared its evolution in subsequent images with the modelled evolution. The pixels of the highest TSM concentration were identified and one particle was released at the centroid of each of the identified pixels. The position of each particle was computed in the particle tracking simulation and compared with the centroid of each pixel processed from remote sensing images for each time step. A tracer test simulation confirmed that the TSM patch was not influenced by TSM input from the Rhône River over the time period considered (see Supplemental Information, Fig. S2). As the Rhône River is the major source of allochthonous TSM, we therefor assume that allochthonous TSM does not influence the simulation results for our area of concern. Furthermore, resuspension in the lake was also neglected as the Reynolds numbers are typically low and do not generate significant shear (Gloor et al., 1994).

For the second scenario, the Rhône River was considered as the major source of TSM in Lake Geneva. TSM was continuously released at the Rhône River inlet from June 28 to 29, 2019, at concentrations positively correlated to the turbidity measurements at the Rhône River estuary (in Supplemental Information, Fig. S3). The plume simulated by the numerical model was then compared with the satellite image taken in the morning of June 29, 2019. In order to mimic the penetration depth of the satellite images, the simulation results included only the particles that were situated less than 10 m deep in the water column. Furthermore, a sensitivity analysis was performed on the dispersion coefficient. Three values of 'a' in equation (4) were chosen to verify the effect of change in magnitude for this dispersion coefficient, whereas the exponential term 'b' was kept as default since this exponential increase of the dispersion coefficient over time and length scale is not addressed in this study.

For the third scenario, particles were released based on the TSM distribution observed across the whole lake. One hundred particles were released in the pixel with the maximum TSM concentration and the number of particles released was scaled down based on the relative concentration of TSM to the maximum TSM concentration. The simulation period lasted from April 15 to 20, 2019. The most distinctive pattern captured by Sentinel-3 images was located in the mid-east part of Lake Geneva during this period, while we masked the western side of the lake in order to avoid cloud buffer artefacts. As in scenario 2, the simulation results included only the particles that were less than 10 m deep in the water column. The features of the TSM patches were compared and a transect across the lake was chosen to validate the simulations' and observations' spatial consistence.

2.6. Interpolation of satellite images from particle tracking simulations

Under cloudy conditions, satellite images can only capture partial information of the area of interest. However, numerical models always provide uninterrupted information both in space and time. We use a simple gain-offset correction method to fill in missing information in images influenced by cloud coverage on particular days. In order to fill in the missing part of the satellite image, the information in the original image remains unchanged while the empty pixels in the satellite image obtain their new values S_n according to the corresponding pixel values in the numerical model P through a linear regression:

$$S_n = R_t{*}P + R_b \tag{5}$$

The coefficients R_t and R_b are obtained from a least square fit from the valid data sets in processed satellite images and in the simulation results. In this manner, the pixels available in partly cloudy satellite images are kept, while cloud gaps are filled with values inferred from numerical simulations to obtain a complete TSM map. To validate this interpolation approach, we manually created gaps in cloud-free images. The inferred TSM in the gaps was then compared with the original TSM estimates from satellite imagery.

3. Results

3.1. Calibration of the sigma-layer hydrodynamic model

The calibrated parameters of the sigma-layer hydrodynamic model, along with the original, validated z-layer model values, are shown in Table 1. The parameters Z_0 was greater than the values from the z- layer model system while C_{HV} and C_{HD} remained close to their default values. Finally, the wind drag coefficients were set to a piecewise linear function instead of a linearly increasing relationship of wind speed (see Supplemental Information, Fig. S4).

3.2. Validation of the sigma-layer hydrodynamic model

The calibrated sigma-layer hydrodynamic model was first validated against surface water temperatures (Fig. 2) and surface velocities (Fig. 3) measured at Buchillon station. Surface water temperature had an increasing trend from April 14 to 20 (Fig. 2a), while the mean surface water temperature remained relatively stable from June 9 to 15 (Fig. 2b). During August 11 to 17, an upwelling event appeared near the lake shore, which caused the surface water temperature to drop continuously (Fig. 2c). Velocity measurements (Fig. 3) revealed that the mean surface velocity was around 0.05 m/s in April and June, whereas the velocity in August was higher, reaching ~ 0.1 m/s. Simulations yielded a good agreement in absolute values and in trends with the observed data for both surface temperature and velocity (Figs. 2 and 3).

We then validated the performance of the sigma-layer hydrodynamic model based on three vertical temperature and velocity profiles measured at the LéXPLORE platform. Fig. 4 shows an example comparison between the 3D simulation and field measurements in the vertical direction obtained in June 2019. The temperature profile reveals that stratification was still in the early developing stage and the velocity dropped rather rapidly from the water surface to a depth of ~ 20 m. The simulations were able to capture these features.

The mean absolute error (MAE) and the root mean square error (RMSE) between the measurements and the simulations were computed for all three profiles, to evaluate the goodness of fit of the numerical model (Table 2). The MAEs of temperature were all below 0.8 °C and the MAEs of velocities were well contained within ~ 0.04 m/s while the temperature and velocity RMSEs were within 1 °C and 0.07 m/s respectively.

3.3. Validation of the particle tracking model

The simulation for an instantaneous point source was run for the period from June 24 to 29, 2019. Ten pixels of the highest TSM concentration in the lake centre was taken as instantaneous release in the simulation. Fig. 5 shows the positions of the high concentration pixels in the centre of the lake obtained from the processed satellite images on June 24 and 29, 2019 (depicted as red dots in Fig. 5a and 5b), compared with the simulated particle tracks shown in close-up in Fig. 5c. The corresponding statistics of the centroids and the particles are given in Table 3.

The visual comparison renders a good agreement between the processed satellite images and the particle tracking simulations. As depicted in Fig. 5, the cloud of patches moved from the centre towards the north shore of Lake Geneva over the course of five days. This transport of TSM was readily observed in the satellite images and was also well captured

Table 1
Original parameters of the z-layer model and calibrated values of the sigma-layer model.

Parameter	Z_0 (m)	C_{HV} (m^2/s)	C_{HD} (m^2/s)	Wind drag coefficients
Z-layer	0.1	1	1	Linearly increasing
Sigma-layer	1.1	1.2	1.2	Piecewise linear function

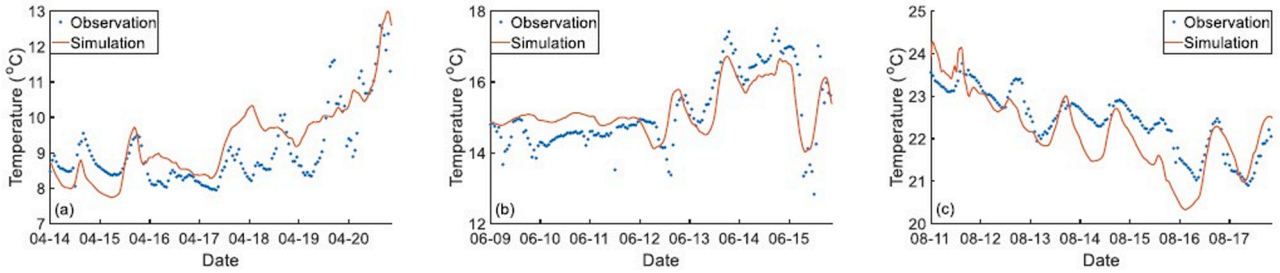

Fig. 2. Comparison between simulation (orange line) and observation (blue dots) of surface water temperatures at Buchillon station for three week-long periods in April (a), June (b) and August (c) 2019.

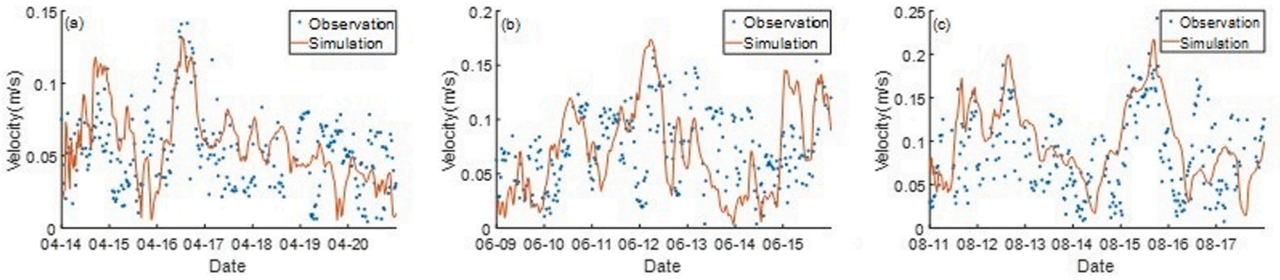

Fig. 3. Comparison between simulation (orange line) and observation (blue dots) of surface velocities at Buchillon station for three week-long periods in April (a), June (b) and August (c) 2019.

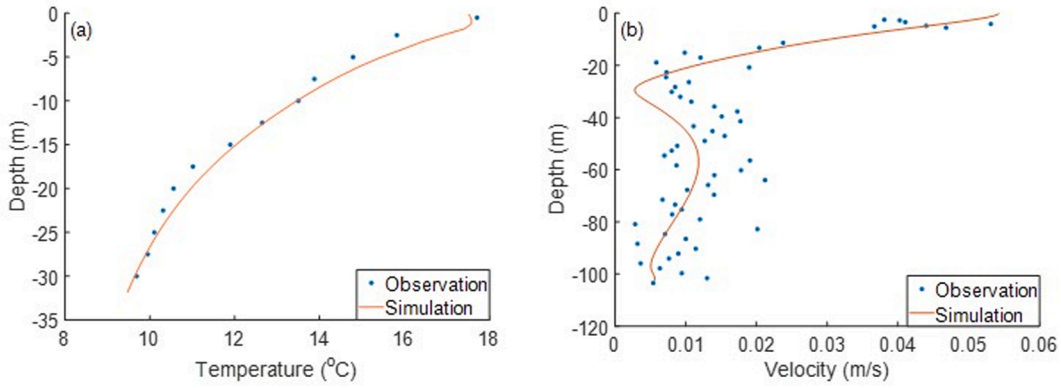

Fig. 4. Comparison of vertical profiles of simulated and observed temperature (a) and velocity (b) at LéXPLORE platform on June 14, 2019.

Table 2
Mean absolute error (MAE) and root mean square error (RMSE) between simulated and measured temperatures and velocity profiles at the LéXPLORE platform.

Parameters	April 2019	June 2019	August 2019	Vertical profile
MAE Temperature (±°C)	0.77	0.67	0.48	0.30
MAE Velocity (±m/s)	0.03	0.04	0.04	0.01
RMSE Temperature (±°C)	0.82	0.71	0.57	0.42
RMSE Velocity (±m/s)	0.04	0.06	0.07	0.02

by the simulated particle movement. Results from the statistics in Table 3 indicated that deviations between the observations and the simulations were in the range of about one to two mesh grids, which is ~ 200 to 400 m. On the fifth day, the observed and simulated centres of the clouds fell within ~ 400 m of each other, which is a short distance given the total path length of ~ 10 km travelled over the course of five days.

In the second case, the particle tracking model was used to capture a continuous source of TSM release at the Rhône River inlet. In Fig. 6, the plume simulated by the particle tracking model is compared with the satellite image taken in the morning of June 29, 2019. The simulated plume agrees qualitatively with the observation from the satellite images with respect to the direction of particle transport, plume size and concentration of TSM. As the simulation results demonstrate, the peak of the modelled plume was at a comparable distance to the mouth of the Rhône River inlet compared to the satellite observation. The main exception is how the simulated particle loads decrease towards zero, where the satellite observes about 3–4 g/m^3 local background concentration. By design, a point source scenario can of course not reproduce such a background concentration.

We used this example to evaluate the influence of the dispersion coefficient on simulation results. Fig. 7 depicts the results when dispersion coefficient constant 'a' (Eq.4) was modified from its Delft3D default value of $a = 1$, used in this study (Fig. 7a), to $a = 0.1$ (Fig. 7b) and to $a = 10$ (Fig. 7c). We conclude that the adjustment of this parameter is essential for conducting realistic Lagrangian studies.

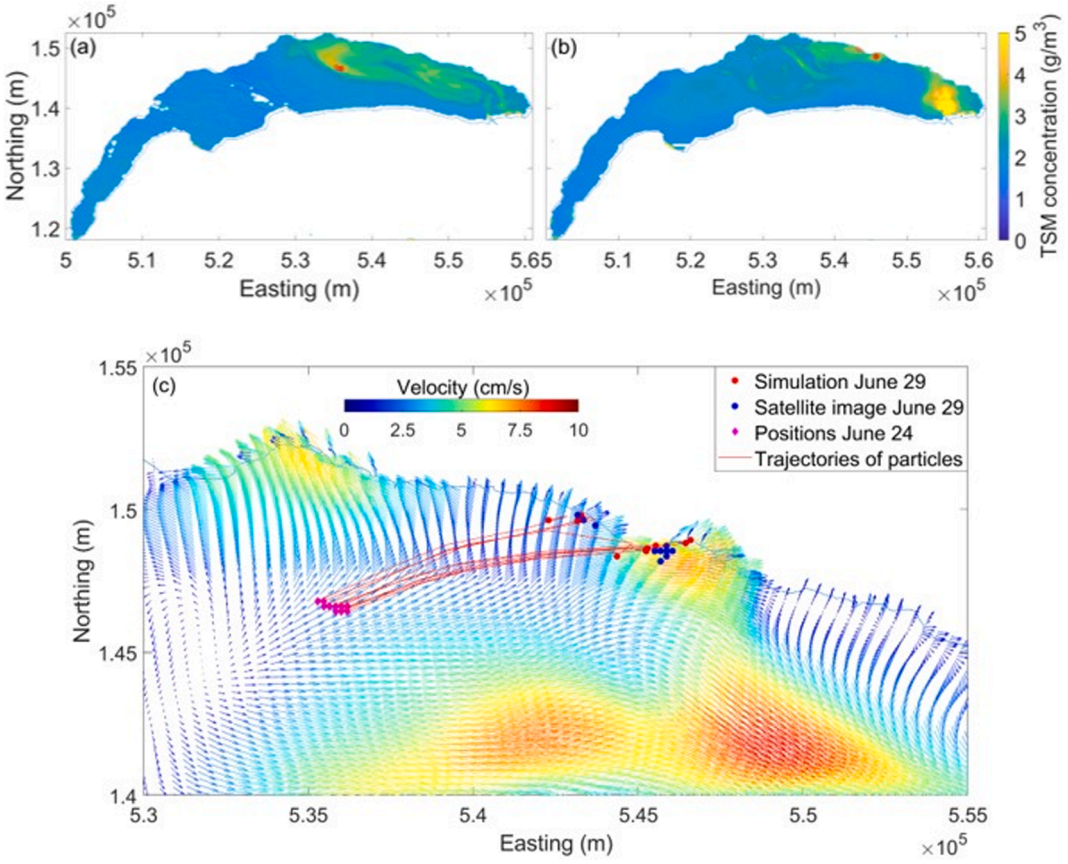

Fig. 5. Comparison of centroids of high concentration pixels obtained from Sentinel-2 images (red dots) on June 24, 2019 (a) and June 29, 2019 (b) with positions of particles throughout particle tracking simulations (c). The burgundy dots in (c) are simulated particle positions on June 24, the red dots represent the simulated final particle positions on June 29 and the blue dots show the high concentration pixels from satellite images on June 29, 2019.

Table 3
Statistics of the centroids of high concentration pixels from the satellite image and the simulated particles.

Date (June 29, 2019)	Sentinel-2 images	Particle tracking	Absolute difference
Centre of X, Easting (m)	545,066	544,690	376
Centre of Y, Northing (m)	148,834	148,760	74
Half major principal axis (m)	1290	1460	170
Half minor principal axis (m)	153	405	251
Characteristic cloud size (m)	1887	3264	1377

The simulation for the entire lake domain lasted from April 15 to 20, 2019. During this period, the transport pattern of the high concentration TSM patches were simulated daily by particle tracking. In contrast, the satellite images were hampered by cloud coverage, thus only data from April 17 to 20 were available.

Fig. 8 illustrates the TSM concentrations obtained through satellite images and the particle tracking simulations. Again, there is a good qualitative match between the observed and simulated concentrations. A plume of high concentration patches of TSM moved from the east part of the lake towards the lake centre, while clinging to the northern shore of Lake Geneva. This pattern of transport was well captured by particle tracking. A splitting of the TSM patches in the open water of Lake Geneva was observed on April 20, and the model partly captured this dynamic behaviour.

In Fig. 9, the observed and simulated TSM concentrations at the virtual sampling transect determined for April 17 to 20, 2019 is illustrated. For both methods and at the entire transect, the TSM concentration fell within the range of 1–2.5 g/m^3 throughout the period considered. The general trend observed at the transect was that the TSM

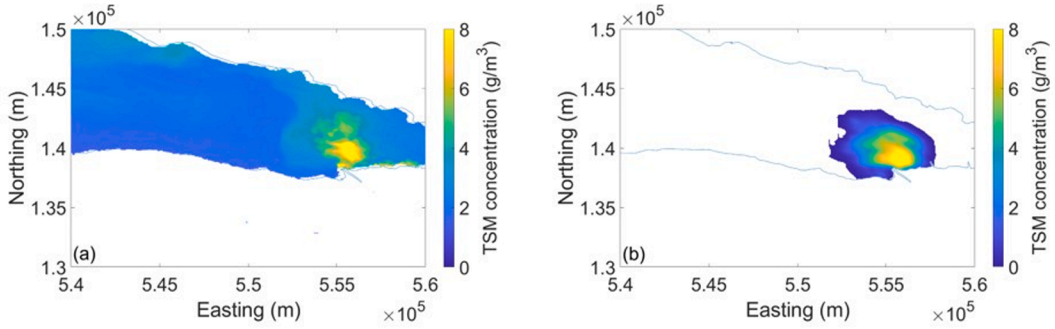

Fig. 6. Plume from the Rhône River processed from satellite images (a) and simulated by the particle tracking model (b) for June 29, 2019.

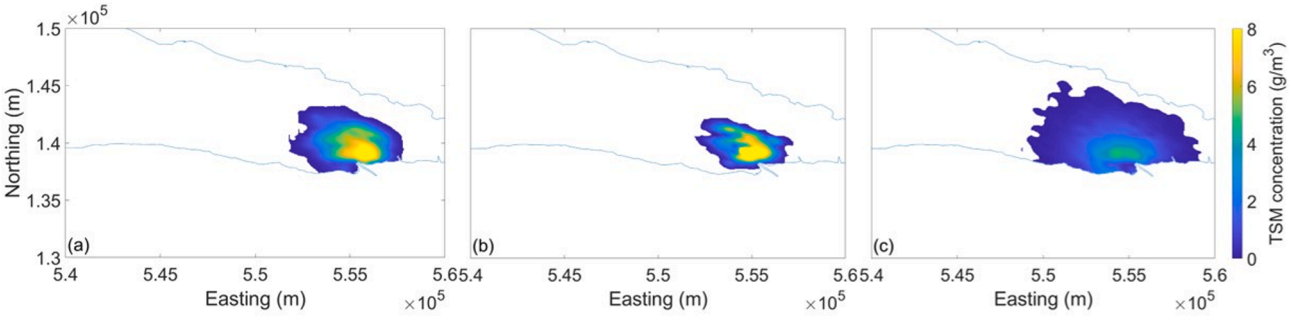

Fig. 7. Sensitivity analysis on the dispersion coefficient constant 'a' (Eq. (4)) with a value of 1 (a), 0.1 (b) and 10 (c).

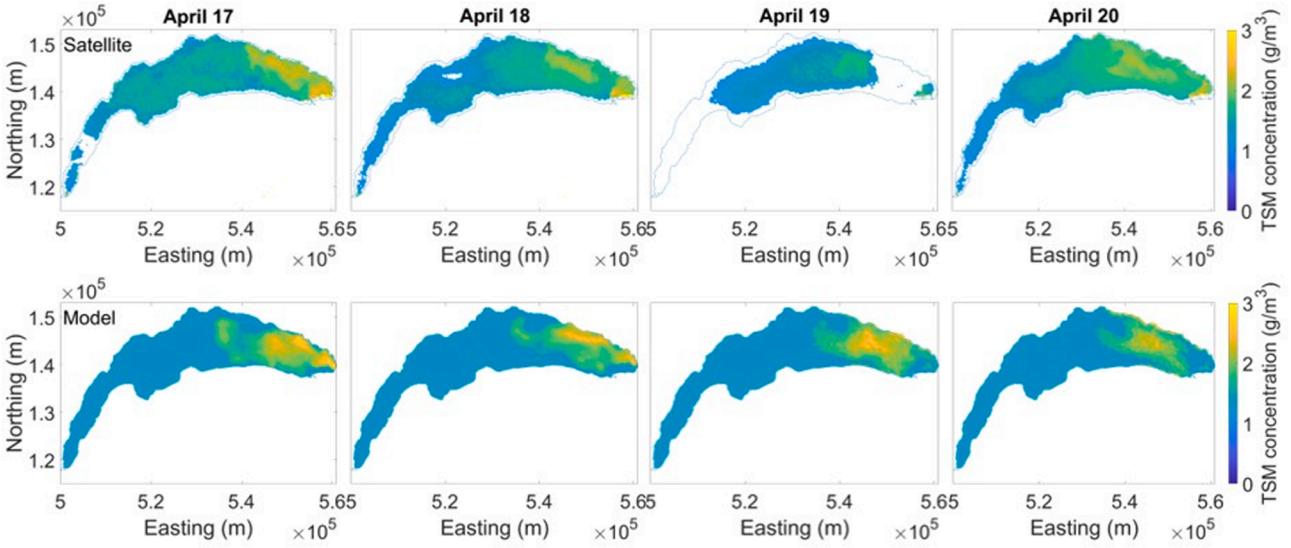

Fig. 8. Concentration of TSM obtained from Sentinel-3 satellite images (top) and the particle tracking model (bottom) from April 17 to 20, 2019, between 10.00 and 11.00 h. On April 19, the satellite image was partly obstructed by clouds.

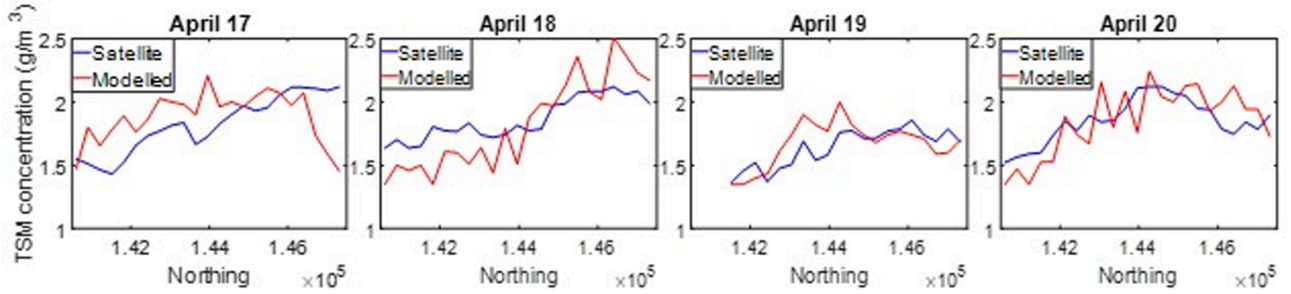

Fig. 9. Concentration of TSM along the virtual sampling transect (Fig. 1) from April 17 to 20, 2019 obtained from both processed satellite images and the particle tracking simulations.

concentration increased on April 18, decreased on April 19 and underwent a small increase on April 20. This may be caused by the western movement of the TSM plume seen in Fig. 8, with high concentration parcels passing the transect on April 17, which led to an increase in the absolute TSM concentrations. After the patches passed through, the concentration dropped again. The increase in TSM on April 20 could result from the splitting of the plume (Fig. 8). Notably, the simulated temporal TSM concentration trends were often in good agreement with the processed remote sensing data for the middle of the transect, while near the boundaries the simulation deviated stronger from the observation. The mean relative error between the TSM concentration obtained from satellite images and the particle tracking simulations along the transect was within ~ 9% while the root mean square error (RMSE) was 0.17 g/m^3 averaged on all four days.

3.4. Interpolation of satellite images from particle tracking simulations

To assess the utility of particle tracking as a method to interpolate between satellite images, we manually impaired the satellite image of April 18, 2019, and subsequently replenished the image using particle tracking simulations. In a first step, we compared the simulation results against the results obtained from the satellite image on April 18 (Fig. 10). Several remotely sensed TSM estimates scatter towards 0 g/m^3, which is neither confirmed by the modelled TSM, nor plausible

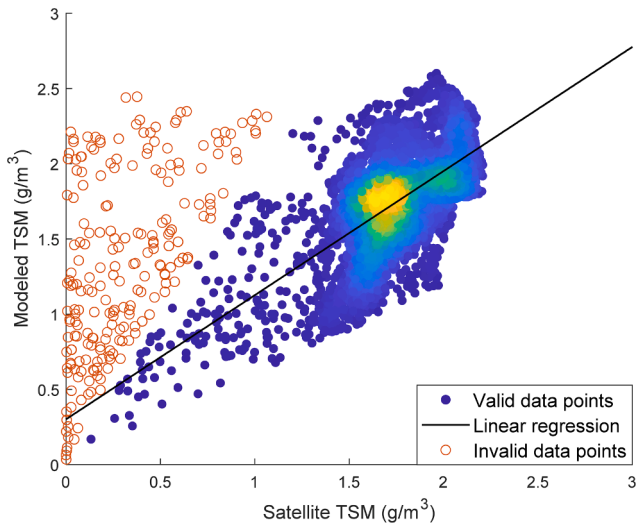

Fig. 10. Comparison of the simulation results against the remote sensing data on April 18, 2019. Linear regression parameters (Eq. (5)) correspond to: R_t = 0.83 and R_b = 0.30.

given that the corresponding pixels are distributed along the lake shore. Land proximity is known to impair remote sensing retrievals (Melet et al., 2020), we therefore remove all pixels with TSM_{Mod} greater than 2* TSM_{Sat} from further analysis. After exclusion of the invalid data points, a linear regression of simulation results versus the remote sensing data yielded a Pearson correlation coefficient of 0.64. The linear regression was then used to fill in missing information on the image where gaps were created manually (Fig. 11). The interpolation yielded a relative abundance of TSM and a position of the TSM plume in the impaired section that corresponded well to the original satellite image. However, the pattern of the TSM patches varied between the original image and the interpolation.

4. Discussion

4.1. The hydrodynamic model captures measurements of water temperature and velocity

The surface temperature and velocity measurements are important in revealing the surface dynamics of the lake. The comparison of the measured surface temperature with those derived from the hydrodynamic model (Fig. 2) indicates that the model captured the trends of the surface temperature changes in the simulation periods and the temperature differences between model and observations were small. The continuous drop of surface temperature in August, shown in Fig. 2c, was likely caused by an upwelling event near the north shore of Lake Geneva, which counteracted the warming effect of the warmer summer air. This specific feature was correctly simulated by the numerical model, which is essential to determine the local temperature conditions. While temperature is important to many lacustrine processes, current velocity is crucial to determine the transport of any substance in lakes. The velocity, illustrated in Fig. 3, shows that the simulation rendered similar results as the ADCP measurements in magnitude and in the tendency of velocity change, for all three simulation periods. The vertical velocity profile shown in Fig. 4 suggests that velocity decreased drastically from the surface to a depth of ~ 20 m and stayed relatively stable at greater depths. This feature, along with the absolute velocities, were also satisfactorily captured by the numerical simulation. The validation by the temperature and velocity data thus confirmed that the hydrodynamic model is sufficiently accurate in simulating the dynamics of Lake Geneva and could serve as a basis for subsequent water quality simulations.

4.2. Particle tracking simulations up to the whole lake domain are confirmed by satellite imagery

The use of a Lagrangian approach is well-suited to predict particle transport in the lake. We here demonstrate that transport predictions by the Lagrangian particle model corresponded well to satellite imagery of TSM for different scenarios. The model accurately predicted the trajectories of particles released instantaneously in the centre of the lake (Fig. 5). It also reproduced the size and the shape of the plume arising from a continuous particle release at the Rhône River (Fig. 6). And finally, the model was also able to quantitatively capture particle transport in the whole lake domain (Fig. 8). Overall, our findings thus indicate that the particle tracking model is competent in simulating the dynamics of passive tracers in Lake Geneva and can serve as a tool for 3D water quality simulation for this deep lake. However, we note that successful simulation is contingent on appropriate calibration of the dispersion coefficient. Specifically, a sensitivity analysis of the dispersion coefficient a (Fig. 7) suggested that the particle tracking simulation with a default value of $a = 1$ was suitable, though this value has a typical uncertainty of half a magnitude (Peeters et al., 1996).

Further improvements in both particle tracking and TSM measurements by satellite may enhance the agreement between measurement and simulation. For example, an increase in TSM in the lake was observed on April 20 (Figs. 8 and 9). While such a feature may arise from plume movement and splitting as hypothesized herein, other possibilities include vertical redistribution or growth of phytoplankton. Such TSM production processes, however, are currently not included in the model. Furthermore, deviations were observed between measurement and simulation near the lake shore (Fig. 9). These deviations may be due to adjacency effects on the remote sensing retrieval method. It is further worth noting that the increased spatial variability in the remotely sensed data is likely due to noise in the observation system, a limitation that can possibly be mitigated by means of spatial aggregation, such as the 3x3 pixel median applied in Fig. S1.

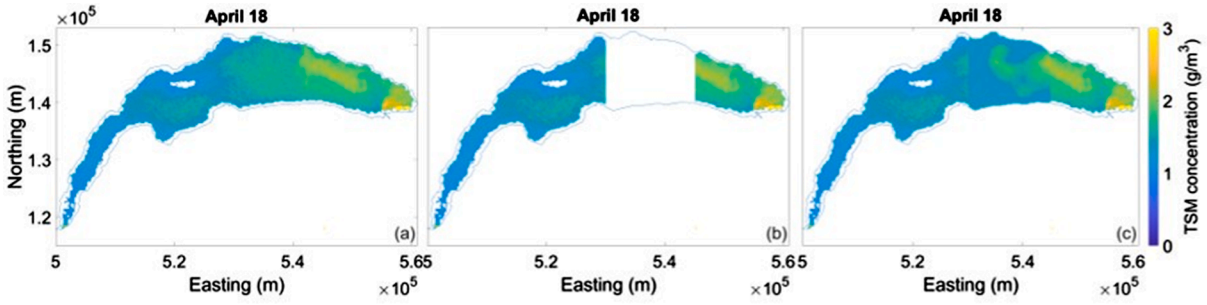

Fig. 11. Original satellite image (a), manually impaired image (b) and the interpolated image (c) on April 18, 2019.

4.3. Particle tracking can complement remote sensing data

When remote sensing techniques and particle tracking are coupled, the two methods can complement one another for greater information gain. A particular strength of the particle tracking is that it provides uninterrupted results in space and time. Once the numerical model is validated, the results can fill in gaps in remote sensing data or serve as a means for interpolation between satellite images. The invalid data points identified in Fig. 10 demonstrate that the numerical model can mitigate potential errors from remote sensing techniques, whereas the valid data points validate the performance of the particle tracking model. As illustrated in Fig. 11, the missing information in the impaired satellite image could be inferred by the particle tracking model to yield a complete picture that is comparable to the original satellite image. In addition, while satellite imagery provides accurate information on the spatial distribution of concerned variables at specific times, it is not feasible to predict future scenarios only based on imaging. However, when coupling satellite imagery with particle tracking, the information from satellite images can be readily translated into particle distributions as initial conditions for the model, to allow estimations of future developments of the movement dynamics.

4.4. Limitations and outlook

The proposed particle tracking model was based on a hydrodynamic model for Lake Geneva. While the hydrodynamic model functions to simulate large scale motions of the lake, it does not solve small scale motions such as mixing processes near the Rhône River inlet. In this study, given the grid size in this model, we assume that the riverine water has lost his momentum in the first grid point and the currents then evolve as a function of the lake dynamic only. A model with finer grid size as well as a flexible horizontal mesh system can help solving small scale dynamics and may elevate the simulation accuracy.

Particle tracking is particularly suitable for near- to mid-field simulations and possesses advantage for the simulation of microorganisms. One successful example is the use of particle tracking to study the fate of infectious hematopoietic necrosis virus among salmon farms on the Discovery Islands region of British Columbia (Foreman et al., 2015). However, microbial water quality simulations rely on the availability of data to parameterize the effect of different environmental processes (e.g., sunlight) on microorganisms. To fully exploit the use of particle tracking to simulate microbial water quality, future work should thus include lab of field experiments to expand the current data set and include a greater variety of targets of interest to the aquatic system.

When combined with remote sensing techniques, (Atwood et al., 2019) demonstrated that satellite-derived images can be combined with particle tracking modelling to track microplastics in the Po River, Italy. In our study, examples investigated highlight the potential of particle tracking to interpolate between two cloud-free satellite overpasses. For instance, the revisit time of Sentinel-2 satellites for Lake Geneva region is around 5 days. Our method allows the 4-day gap of two consecutive sentinel-2 images to be filled with results from numerical simulations. In future work, the algorithm to complete the image filling process with numerical simulations could be further refined by implementing more complex interpolation methods than the simple linear regression method applied in this study.

Despite the remaining shortcomings, all these studies indicate that particle tracking and remote sensing techniques are important and powerful tools in resolving environmental processes occurring in the aquatic systems. Improvement in the accuracy of numerical simulations, a more universal parameter retrieval method for satellite images and polished algorithms to connect simulation results and satellite image derived quantities are desired to further exploit the synergy between particle tracking simulations and remote sensing techniques.

5. Conclusions

Remote sensing has broad and diverse applications in monitoring lake hydrology, hydrodynamics and water quality, with the advantage of large spatial coverage and accurate mapping of parameters of interest. Yet the nature of satellite sensing fails to provide three-dimensional data output of real-time observations for deep lakes. On the other hand, numerical models can provide uninterrupted three-dimensional evolution for hydrodynamic and water quality parameters. However, such models are usually complex and difficult to apply due to the lack of data for model calibration and validation.

In this study, we set up a hydrodynamic and a subsequent particle tracking model for Lake Geneva and examined the validation of such a model by remote sensing techniques. We demonstrated that using satellite images as observational data for validation of such particle tracking models is applicable and robust. The model, in return, provided the possibility for data interpolation and inference for remote sensing techniques to fill gaps between two snapshots, or to remedy data gaps due to cloud coverage in satellite images. The combination of remote sensing and particle tracking simulations thus provides a greater information depth than the sum of its part, and can markedly improve the understanding and the prediction of processes occurring in lakes. Given its Lagrangian basis, the particle tracking model can be readily adapted to simulate concentrations of microorganisms with self-dependent movement and die-off processes. It is thus a powerful tool for future microbial water quality modelling. The combination of remote sensing techniques and particle tracking water quality modelling promises a future with more accurate, real-time and flexible lake monitoring and modelling practices and thus facilitate decision making on water resources and environmental management.

Data statement.

Data and code will be made available on Zenodo upon acceptance of the manuscript.

CRediT authorship contribution statement

Chaojie Li: Conceptualization, Methodology, Software, Validation, Formal analysis, Investigation, Data curation, Writing – original draft, Writing – review & editing, Visualization. **Daniel Odermatt:** Conceptualization, Methodology, Software, Investigation, Data curation, Writing – review & editing. **Damien Bouffard:** Conceptualization, Writing – review & editing. **Alfred Wüest:** Conceptualization, Writing – review & editing, Supervision. **Tamar Kohn:** Conceptualization, Resources, Writing – original draft, Writing – review & editing, Supervision, Project administration, Funding acquisition.

Declaration of Competing Interest

The authors declare that they have no known competing financial interests or personal relationships that could have appeared to influence the work reported in this paper.

Acknowledgements

The authors thank the French Alpine Lakes Observatory (SOERE-OLA) for providing data from © SOERE OLA-IS, AnaEE-France, INRA Thonon-les-Bains.

Funding

This work was supported by the Swiss National Science (grant no. 31003A_182468).

Appendix A. Supplementary data

Supplementary data to this article can be found online at https://doi.

org/10.1016/j.jag.2022.102809.

References

Allan, M.G., Hamilton, D.P., Trolle, D., Muraoka, K., McBride, C., 2016. Spatial heterogeneity in geothermally-influenced lakes derived from atmospherically corrected Landsat thermal imagery and three-dimensional hydrodynamic modelling. Int. J. Appl. Earth Obs. Geoinf. 50, 106–116. https://doi.org/10.1016/j.jag.2016.03.006.

Aschbacher, J., Milagro-Pérez, M.P., 2012. The European Earth monitoring (GMES) programme: Status and perspectives. Remote Sens. Environ. 120, 3–8. https://doi.org/10.1016/j.rse.2011.08.028.

Atwood, E.C., Falcieri, F.M., Piehl, S., Bochow, M., Matthies, M., Franke, J., Carniel, S., Sclavo, M., Laforsch, C., Siegert, F., 2019. Coastal accumulation of microplastic particles emitted from the Po River, Northern Italy: Comparing remote sensing and hydrodynamic modelling with in situ sample collections. Mar. Pollut. Bull. 138, 561–574. https://doi.org/10.1016/j.marpolbul.2018.11.045.

Baracchini, T., Chu, P.Y., Šukys, J., Lieberherr, G., Wunderle, S., Wüest, A., Bouffard, D., 2020a. Data assimilation of in situ and satellite remote sensing data to 3D hydrodynamic lake models: a case study using Delft3D-FLOW v4.03 and OpenDA v2.4. Geosci. Model Dev. 13, 1267–1284. https://doi.org/10.5194/gmd-13-1267-2020.

Baracchini, T., Wüest, A., Bouffard, D., 2020b. Meteolakes: An operational online three-dimensional forecasting platform for lake hydrodynamics. Water Res. 172, 115529. https://doi.org/10.1016/j.watres.2020.115529.

Bonnet, M.P., Poulin, M., Devaux, J., 2000. Numerical modeling of thermal stratification in a lake reservoir. Methodology and case study. Aquat. Sci. 62, 105–124. https://doi.org/10.1007/s000270050001.

Bouffard, D., Kiefer, I., Wüest, A., Wunderle, S., Odermatt, D., 2018. Are surface temperature and chlorophyll in a large deep lake related? An analysis based on satellite observations in synergy with hydrodynamic modelling and in-situ data. Remote Sens. Environ. 209, 510–523. https://doi.org/10.1016/j.rse.2018.02.056.

Chen, X., Lu, J., Cui, T., Jiang, W., Tian, L., Chen, L., Zhao, W., 2010. Coupling remote sensing retrieval with numerical simulation for SPM study-Taking Bohai Sea in China as a case. Int. J. Appl. Earth Obs. Geoinf. 12, S203–S211. https://doi.org/10.1016/j.jag.2009.10.002.

Curtarelli, M.P., Alcântara, E.H., Rennó, C.D., Stech, J.L., 2014. Physical changes within a large tropical hydroelectric reservoir induced by wintertime cold front activity. Hydrol. Earth Syst. Sci. 18, 3079–3093. https://doi.org/10.5194/hess-18-3079-2014.

Delft3D-Flow. User Man. 712.

Donlon, C., Berruti, B., Buongiorno, A., Ferreira, M.H., Féménias, P., Frerick, J., Goryl, P., Klein, U., Laur, H., Mavrocordatos, C., Nieke, J., Rebhan, H., Seitz, B., Stroede, J., Sciarra, R., 2012. The Global Monitoring for Environment and Security (GMES) Sentinel-3 mission. Remote Sens. Environ. 120, 37–57. https://doi.org/10.1016/j.rse.2011.07.024.

Dörnhöfer, K., Oppelt, N., 2016. Remote sensing for lake research and monitoring - Recent advances. Ecol. Indic. 64, 105–122. https://doi.org/10.1016/j.ecolind.2015.12.009.

Drusch, M., Del Bello, U., Carlier, S., Colin, O., Fernandez, V., Gascon, F., Hoersch, B., Isola, C., Laberinti, P., Martimort, P., Meygret, A., Spoto, F., Sy, O., Marchese, F., Bargellini, P., 2012. Sentinel-2: ESA's Optical High-Resolution Mission for GMES Operational Services. Remote Sens. Environ. 120, 25–36. https://doi.org/10.1016/j.rse.2011.11.026.

Foreman, M.G.G., Guo, M., Garver, K.A., Stucchi, D., Chandler, P., Wan, D., Morrison, J., Tuele, D., 2015. Modelling infectious hematopoietic necrosis virus dispersion from marine salmon farms in the Discovery Islands, British Columbia, Canada. PLoS One 10, 1–25. 10.1371/journal.pone.0130951.

Foster, I.D.L., Millington, R., Grew, R.G., 1992. The impact of particle size controls on stream turbidity measurement; some implications for suspended sediment yield estimation. Eros. sediment Monit. Program. river basins. Proc. Int. Symp. Oslo 1992, 51–62.

Gholizadeh, M., Melesse, A., Reddi, L., 2016. A comprehensive review on water quality parameters estimation using remote sensing techniques. Sensors (Switzerland) 16 (8), 1298. https://doi.org/10.3390/s16081298.

Gloor, M., Wüest, A., Münnich, M., 1994. Benthic boundary mixing and resuspension induced by internal seiches. Hydrobiologia 284 (1), 59–68. https://doi.org/10.1007/BF00005731.

Hoyer, A.B., Schladow, S.G., Rueda, F.J., 2015. A hydrodynamics-based approach to evaluating the risk of waterborne pathogens entering drinking water intakes in a large, stratified lake. Water Res. 83, 227–236. https://doi.org/10.1016/j.watres.2015.06.014.

Kiefer, I., Odermatt, D., Anneville, O., Wüest, A., Bouffard, D., 2015. Application of remote sensing for the optimization of in-situ sampling for monitoring of phytoplankton abundance in a large lake. Sci. Total Environ. 527–528, 493–506. https://doi.org/10.1016/j.scitotenv.2015.05.011.

Lehmann, M.K., Schütt, E.M., Hieronymi, M., Dare, J., Krasemann, H., 2021. Analysis of recurring patchiness in satellite-derived chlorophyll a to aid the selection of representative sites for lake water quality monitoring. Int. J. Appl. Earth Obs. Geoinf. 104, 102547. https://doi.org/10.1016/j.jag.2021.102547.

Liu, Y.Y., Weisberg, R.H.R.H., Hu, C.C., Zheng, L.L., 2011. Trajectory Forecast as a Rapid Response to the Deepwater Horizon Oil Spill. Monit. Model. Deep. Horiz. Oil Spill A Rec. Enterp., Geophysical Monograph Series. 10.1029/2011GM001121.

Melet, A., Teatini, P., Le Cozannet, G., Jamet, C., Conversi, A., Benveniste, J., Almar, R., 2020. Earth Observations for Monitoring Marine Coastal Hazards and Their Drivers. Surv. Geophys. 41 (6), 1489–1534. https://doi.org/10.1007/s10712-020-09594-5.

Neukermans, G., Ruddick, K., Loisel, H., Roose, P., 2012. Optimization and quality control of suspended particulate matter concentration measurement using turbidity measurements. Limnol. Oceanogr. Methods 10 (12), 1011–1023. https://doi.org/10.4319/lom.2012.10.1011.

Nouchi, V., Kutser, T., Wüest, A., Müller, B., Odermatt, D., Baracchini, T., Bouffard, D., 2019. Resolving biogeochemical processes in lakes using remote sensing. Aquat. Sci. 81, 1–13. https://doi.org/10.1007/s00027-019-0626-3.

Nouchi, V., Odermatt, D., Wüest, A., Bouffard, D., 2018. Effects of non-uniform vertical constituent profiles on remote sensing reflectance of oligo- to mesotrophic lakes. Eur. J. Remote Sens. 51 (1), 808–821. https://doi.org/10.1080/22797254.2018.1493360.

Odermatt, D., Gitelson, A., Brando, V.E., Schaepman, M., 2012. Review of constituent retrieval in optically deep and complex waters from satellite imagery. Remote Sens. Environ. 118, 116–126. https://doi.org/10.1016/j.rse.2011.11.013.

Park, S., Western, L.M., Saito, T., Redington, A.L., Henne, S., Fang, X., Prinn, R.G., Manning, A.J., Montzka, S.A., Fraser, P.J., Ganesan, A.L., Harth, C.M., Kim, J., Krummel, P.B., Liang, Q., Mühle, J., O'Doherty, S., Park, H., Park, M.-K., Reimann, S., Salameh, P.K., Weiss, R.F., Rigby, M., 2021. A decline in emissions of CFC-11 and related chemicals from eastern China. Nature 590 (7846), 433–437. https://doi.org/10.1038/s41586-021-03277-w.

Peeters, F., Wüest, A., Piepke, G., Imboden, D.M., 1996. Horizontal mixing in lakes. J. Geophys. Res. C Ocean. 101 (C8), 18361–18375. https://doi.org/10.1029/96JC01145.

Piccolroaz, S., Amadori, M., Toffolon, M., Dijkstra, H.A., 2019. Importance of planetary rotation for ventilation processes in deep elongated lakes: Evidence from Lake Garda (Italy). Sci. Rep. 9, 1–11. https://doi.org/10.1038/s41598-019-44730-1.

Platzek, F.W., Stelling, G.S., Jankowski, J.A., Pietrzak, J.D., 2014. Accurate vertical profiles of turbulent flow in z-layer models. Water Resour. Res. 50 (3), 2191–2211. https://doi.org/10.1002/2013WR014411.

Razmi, A.M., Barry, D.A., Lemmin, U., Bonvin, F., Kohn, T., Bakhtyar, R., 2014. Direct effects of dominant winds on residence and travel times in the wide and open lacustrine embayment: Vidy Bay (Lake Geneva, Switzerland). Aquat. Sci. 76 (S1), 59–71. https://doi.org/10.1007/s00027-013-0321-8.

Soulignac, F., Danis, P.-A., Bouffard, D., Chanudet, V., Dambrine, E., Guénand, Y., Harmel, T., Ibelings, B.W., Trevisan, D., Uittenbogaard, R., Anneville, O., 2018. Using 3D modeling and remote sensing capabilities for a better understanding of spatio-temporal heterogeneities of phytoplankton abundance in large lakes. J. Great Lakes Res. 44 (4), 756–764. https://doi.org/10.1016/j.jglr.2018.05.008.

Steinmetz, F., Deschamps, P.-Y., Ramon, D., 2011. Atmospheric correction in presence of sun glint: application to MERIS. Opt. Express 19 (10), 9783. https://doi.org/10.1364/OE.19.009783.

Steinmetz, F., Ramon, D., 2018. Sentinel-2 MSI and Sentinel-3 OLCI consistent ocean colour products using POLYMER. Proc. SPIE 13. https://doi.org/10.1117/12.2500232.

Stroud, J.R., Lesht, B.M., Schwab, D.J., Beletsky, D., Stein, M.L., 2009. Assimilation of satellite images into a sediment transport model of Lake Michigan. Water Resour. Res. 45, 1–16. https://doi.org/10.1029/2007WR006747.

Thomas, R.Q., Figueiredo, R.J., Daneshmand, V., Bookout, B.J., Puckett, L.K., Carey, C. C., 2020. A Near-Term Iterative Forecasting System Successfully Predicts Reservoir Hydrodynamics and Partitions Uncertainty in Real Time. Water Resour. Res. 56 (11) https://doi.org/10.1029/2019WR026138.

Vantrepotte, V., Loisel, H., Mériaux, X., Neukermans, G., Dessailly, D., Jamet, C., Gensac, E., Gardel, A., 2011. Seasonal and inter-annual (2002–2010) variability of the suspended particulate matter as retrieved from satellite ocean color sensor over the French Guiana coastal waters. J. Coast. Res. 1750–1754.

Verpoorter, C., Kutser, T., Seekell, D.A., Tranvik, L.J., 2014. A global inventory of lakes based on high-resolution satellite imagery. Geophys. Res. Lett. 41 (18), 6396–6402. https://doi.org/10.1002/2014GL060641.

Watanabe, F., Alcântara, E., Curtarelli, M., Kampel, M., Stech, J., 2018. Landsat-based remote sensing of the colored dissolved organic matter absorption coefficient in a tropical oligotrophic reservoir. Remote Sens. Appl. Soc. Environ. 9, 82–90. https://doi.org/10.1016/j.rsase.2017.12.004.

Wen, Z., Song, K., Shang, Y., Zhao, Y., Fang, C., Lyu, L., 2018. Differences in the distribution and optical properties of DOM between fresh and saline lakes in a semi-arid area of Northern China. Aquat. Sci. 80, 1–12. https://doi.org/10.1007/s00027-018-0572-5.

Wilson, J.D., Sawford, B.L., 1996. Review of Lagrangian stochastic models for trajectories in the turbulent atmosphere. Boundary-Layer Meteorol. 78 (1-2), 191–210. https://doi.org/10.1007/BF00122492.

Wüest, A., Bouffard, D., Guillard, J., Ibelings, B.W., Lavanchy, S., Perga, M.-E., Pasche, N., 2021. LéXPLORE – a floating laboratory on Lake Geneva offering unique lake research opportunities. WIREs Water 8. https://doi:10.1002/wat2.1544.

Wynne, T.T., Stumpf, R.P., Tomlinson, M.C., Fahnenstiel, G.L., Dyble, J., Schwab, D.J., Joshi, S.J., 2013. Evolution of a cyanobacterial bloom forecast system in western Lake Erie: Development and initial evaluation. J. Great Lakes Res. 39, 90–99. https://doi.org/10.1016/j.jglr.2012.10.003.

Xue, P., Schwab, D.J., Sawtell, R.W., Sayers, M.J., Shuchman, R.A., Fahnenstiel, G.L., 2017. A particle-tracking technique for spatial and temporal interpolation of satellite images applied to Lake Superior chlorophyll measurements. J. Great Lakes Res. 43 (3), 1–13. https://doi.org/10.1016/j.jglr.2017.03.012.

Zhou, Q., Wang, W., Huang, L., Zhang, Y., Qin, J., Li, K., Chen, L., 2019. Spatial and temporal variability in water transparency in Yunnan Plateau lakes. China. Aquat. Sci. 81, 1–14. https://doi.org/10.1007/s00027-019-0632-5.